Molecular Biology of the Cell
Vol. 16, 5127–5140, November 2005

Live Imaging of *Drosophila* Brain Neuroblasts Reveals a Role for Lis1/Dynactin in Spindle Assembly and Mitotic Checkpoint Control[V]

Karsten H. Siller,* Madeline Serr,† Ruth Steward,‡ Tom S. Hays,† and Chris Q. Doe*

*Howard Hughes Medical Institute and Institutes of Neuroscience and Molecular Biology, University of Oregon, Eugene, OR 97403; †Department of Genetics, Cell Biology, and Development, University of Minnesota, Minneapolis, MN 55455; and ‡Department of Molecular Biology and Biochemistry, Rutgers University, Piscataway, NJ 08854

Submitted April 22, 2005; Revised July 8, 2005; Accepted August 10, 2005
Monitoring Editor: Erika Holzbaur

Lis1 is required for nuclear migration in fungi, cell cycle progression in mammals, and the formation of a folded cerebral cortex in humans. Lis1 binds dynactin and the dynein motor complex, but the role of Lis1 in many dynein/dynactin-dependent processes is not clearly understood. Here we generate and/or characterize mutants for *Drosophila* Lis1 and a dynactin subunit, Glued, to investigate the role of Lis1/dynactin in mitotic checkpoint function. In addition, we develop an improved time-lapse video microscopy technique that allows live imaging of GFP-Lis1, GFP-Rod checkpoint protein, green fluorescent protein (GFP)-labeled chromosomes, or GFP-labeled mitotic spindle dynamics in neuroblasts within whole larval brain explants. Our mutant analyses show that Lis1/dynactin have at least two independent functions during mitosis: first promoting centrosome separation and bipolar spindle assembly during prophase/prometaphase, and subsequently generating interkinetochore tension and transporting checkpoint proteins off kinetochores during metaphase, thus promoting timely anaphase onset. Furthermore, we show that Lis1/dynactin/dynein physically associate and colocalize on centrosomes, spindle MTs, and kinetochores, and that regulation of Lis1/dynactin kinetochore localization in *Drosophila* differs from both *Caenorhabditis elegans* and mammals. We conclude that Lis1/dynactin act together to regulate multiple, independent functions in mitotic cells, including spindle formation and cell cycle checkpoint release.

INTRODUCTION

An essential step during mitotic cell division involves the equal partitioning of the genetic material between both daughter cells. Correct chromosome segregation requires attachment of microtubules (MTs) emanating from spindle poles to kinetochores, multiprotein complexes assembled on centromeres of chromatids (reviewed in Cleveland *et al.*, 2003). Importantly, sister kinetochores must be attached to MTs originating from opposite spindle poles, a configuration referred to as bipolar attachment, before sister chromatid separation and anaphase onset. A surveillance mechanism termed the "mitotic checkpoint" or "spindle assembly checkpoint" delays anaphase onset and sister chromatid separation until all chromatid pairs are attached and tension is generated between sister chromatids (reviewed in Cleveland *et al.*, 2003; Taylor *et al.*, 2004).

This article was published online ahead of print in *MBC in Press* (http://www.molbiolcell.org/cgi/doi/10.1091/mbc.E05–04–0338) on August 17, 2005.

[V] The online version of this article contains supplemental material at *MBC Online* (http://www.molbiolcell.org).

Address correspondence to: Chris Q. Doe (cdoe@uoneuro.uoregon.edu).

Abbreviations used: MT, microtubule; kMT, kinetochore microtubule; NEB, nuclear envelope breakdown; ALH, after larval hatching; G1, Glued; MTOC, microtubule organizing center.

Components of the mitotic checkpoint were first identified in budding yeast and include the Mad1, Mad2, Mad3, Bub1, and Bub3 proteins (Hoyt *et al.*, 1991; Li and Murray, 1991). Although the Mad and Bub proteins are highly conserved from yeast to human, additional checkpoint proteins including members of the Rough-deal/Zeste-white10 (Rod/Zw10) complex have been identified in higher eukaryotes (Starr *et al.*, 1997; Basto *et al.*, 2000; Chan *et al.*, 2000; Scaerou *et al.*, 2001; Williams *et al.*, 2003). Similar to disruption of Mad or Bub protein function, interference with Rod or Zw10 function abrogates mitotic checkpoint function, promoting chromosome segregation defects due to premature anaphase onset before bipolar chromosome attachment (Karess and Glover, 1989; Williams *et al.*, 1992; Basto *et al.*, 2000; Chan *et al.*, 2000).

Several observations revealed the central role of kinetochores in checkpoint signaling. Functional kinetochores are required for generation of the mitotic checkpoint signal (Rieder *et al.*, 1995), and checkpoint proteins such as Mad2 and Rod are localized to unattached kinetochores (reviewed in Cleveland *et al.*, 2003; Taylor *et al.*, 2004). The Rod/Zw10 complex promotes recruitment of Mad2 to unattached kinetochores (Buffin *et al.*, 2005; Kops *et al.*, 2005). At unattached kinetochores Mad2 is thought to be converted into an "active" species and subsequently released into the cytoplasm where it indirectly inhibits the "anaphase promoting complex/cyclosome" (APC/C). Inhibition of the APC/C in turn prevents premature sister chromatid separation and anaphase onset. At the end of metaphase (after correct bipolar

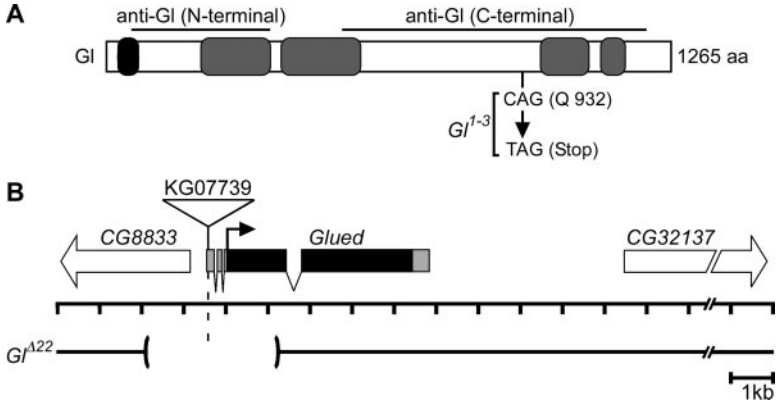

Figure 1. Generation and characterization of *Glued* alleles. (A) Schematic representation of structural domains within the Glued (Gl) protein as predicted by the SMART algorithm: black box: cytoskeleton-associated protein-Glycine (CAP-Gly) MT-binding motif; gray boxes: coiled-coil domains. Also shown is the point mutation in Gl^{1-3} converting codon 932 (CAG) into a premature stop codon. (B) Schematic representation of the *Glued* gene and neighboring annotated genes *CG8833* and *CG32137*. Black boxes: *Glued* coding region; gray boxes: untranslated regions; black arrow: translational start site; dashed line: insertion site of the P-element *l(3)KG07739*. Open brackets indicate the extent of the deletion in the $Gl^{\Delta 22}$ allele generated by imprecise excision of the *l(3)KG07739* P-element. We also obtained viable lines with precise P-element excision, indicating that lethality in $Gl^{\Delta 22}$ is due to the indicated deletion. Homozygous Gl^{1-3}, homozygous $Gl^{\Delta 22}$, and transheterozygous $Gl^{1-3}/Gl^{\Delta 22}$ mutant neuroblasts show indistinguishable phenotypes. The function of the gene *CG8833* is unknown.

MT attachment of all chromatid pairs is achieved), the mitotic checkpoint is inactivated, leading to increased APC/C activity which consequently triggers initiation of sister chromatid separation and anaphase onset (reviewed in Cleveland *et al.*, 2003; Taylor *et al.*, 2004). Insights into the mechanism of checkpoint inactivation in metazoans came from the following observations in mammalian tissue culture and *Drosophila* cells. After MT-attachment, Mad2 and Rod stream off kinetochores along kinetochore MTs (kMTs), resulting in the reduction of kinetochore-associated Mad2 and Rod levels (Howell *et al.*, 2000; Basto *et al.*, 2004). Interference with the function of dynein, a minus end-directed MT-based motor complex that also localizes to unattached kinetochores, causes accumulation of the Mad2 and Rod proteins on attached metaphase kinetochores by blocking their poleward transport and delays metaphase-to-anaphase transition (Howell *et al.*, 2001; Wojcik *et al.*, 2001). These observations led to the model that dynein-dependent poleward transport of checkpoint proteins contributes to silencing of the mitotic checkpoint signal and thereby promotes timely initiation of anaphase.

Despite these recent advances, one area of active research is the identification of dynein-associated proteins contributing to its checkpoint function. One protein shown to physically interact with dynein is the WD40 repeat containing Lis1 protein (Faulkner *et al.*, 2000; Smith *et al.*, 2000; Tai *et al.*, 2002). Mutations in the human *Lis1* gene have been identified as the cause of lissencephaly (Reiner *et al.*, 1993), a condition characterized by severe neurodevelopmental defects as a consequence of abnormal neuronal migration and perhaps neural precursor cell divisions (reviewed in Feng and Walsh, 2001; Vallee *et al.*, 2001). The role of Lis1 in dynein-dependent cellular processes is not clearly understood. For example, dynein is required for pericentrosomal Golgi positioning (reviewed in Karki and Holzbaur, 1999), yet there are conflicting reports whether Lis1 is involved in this process (Faulkner *et al.*, 2000; Smith *et al.*, 2000). The role of Lis1 in cell cycle timing and mitotic checkpoint signaling is also unclear. Injection of Lis1 function-blocking antibodies in mammalian cells led to kinetochore-MT attachment defects and prolonged prometaphase, but no delay in metaphase-to-anaphase transition was observed (Faulkner *et al.*, 2000). These data suggest that Lis1 regulates chromosome alignment rather than contributing to dynein-dependent mitotic checkpoint inactivation. Thus, although Lis1 protein is highly conserved from yeast to man, functional evidence for a role in mitotic checkpoint signaling is minimal.

The evolutionarily conserved dynactin complex also associates with dynein, increases the processivity of the dynein motor (King and Schroer, 2000) and is thought to mediate dynein attachment to its cargo (reviewed in Schroer, 2004). Dynactin recruits dynein to kinetochores (Echeverri *et al.*, 1996) and is required for poleward Mad2 transport and timely anaphase onset in mammalian cells (Howell *et al.*, 2001). However, the role of dynactin in checkpoint signaling has not been investigated in *Drosophila* because of lack of suitable mutant alleles.

Here we report a detailed functional analysis of Lis1 and dynactin in *Drosophila* larval neuroblasts, using an improved time-lapse video microscopy technique that allows live imaging of the neuroblast cell cycle in whole larval brain explants. We show that Lis1 and dynactin are required for centrosome separation and spindle assembly during prophase/prometaphase and contribute to timely metaphase-to-anaphase transition by promoting efficient mitotic checkpoint inactivation. In addition, we describe the subcellular localization of Lis1 and dynactin in mitotic neuroblasts, providing evidence that, in contrast to their homologous proteins in mammals and *Caenorhabditis elegans*, *Drosophila* Lis1 and dynactin localize to kinetochores in a codependent manner.

MATERIALS AND METHODS

Fly Genetics

Oregon R or *y w* flies were used as wild-type controls. Other fly strains used include *FRTG13* $Lis1^{G10.14}$*/CyO* (Liu *et al.*, 1999); $Lis1^{k13209}$*/CyO*; *l(3)KG07739*; *Df(3L)fz-GF3b* (Bloomington Stock Center); $rod^{H4.8}$*/TM6B* (Karess and Glover, 1989); *p[w+ GFP-Rod]* rod^{X5} *e ca* (Scaerou *et al.*, 1999; Basto *et al.*, 2004); *p[w+mC = His2AvT:Avic\GFP-S65T]62A* expressing His2AvD-GFP (Clarkson and Saint, 1999); the gene trap line *G147*, which expresses a green fluorescent protein (GFP)-tagged MT-associated protein (Morin *et al.*, 2001). All mutant alleles were rebalanced over *CyO actin-GFP* or *TM3 actin-GFP Ser*. Newly hatched mutant larvae were identified based on the absence of GFP expression in the gut. Larvae were aged to the late 2nd instar stage (wild type, $Lis1^{-}$, $Lis1^{-}$ $rod^{H4.8}$, $rod^{H4.8}$ 48 h after larval hatching (ALH); *Gl* mutants: 96–120 h ALH) for all phenotypic analyses.

Generation and Characterization of Glued Alleles

We generated a new *Glued* allele, $Gl^{\Delta 22}$, by imprecise excision of the P-element *l(3)KG07739* inserted into the 5′-UTR encoding region of the *Glued* gene (Bellen *et al.*, 2004). PCR and sequence analysis revealed that $Gl^{\Delta 22}$ contains a ~3.2-kb deletion removing the presumptive transcriptional start site of the *Glued* gene (Figure 1B). In addition, the molecular nature of the Gl^{1-3} allele (Harte and Kankel, 1982) was determined by sequence comparison of genomic DNA amplified from homozygous Gl^{1-3} mutant and *Oregon R* larvae using standard PCR techniques, revealing a point mutation converting codon 932 into a premature stop codon (Figure 1A). Homozygous Gl^{1-3}, homozy-

gous $Gl^{\Delta 22}$, and hemizygous $Gl^{1-3}/Df(3L)fz\text{-}GF3b$ animals die as 2nd instar larvae.

Generation of Transgenic Fly Lines Expressing GFP-tagged Lis1 Protein

The complete Lis1 coding sequence was amplified from *Drosophila* EST RE28987 and subcloned into the pUAST vector downstream of, and in-frame with, three repeats encoding EmeraldGFP (Tsien, 1998). Transgenic flies were generated by standard methods. GFP-Lis1 was expressed in larval neuroblasts by crossing pUAST-3xEmeraldGFP-Lis1 transgenic flies to a *worniu-Gal4* driver line (Albertson *et al.*, 2004; see Figure 10 and Supplementary Movie 10). In addition, one of us (R.S.) subcloned the Lis1 coding sequence into the pUASP vector downstream of a single GFP coding sequence; this GFP-Lis1 was ubiquitously expressed in embryos using the maternal *nanos-Gal4* driver for the immunoprecipitation experiments (see Figure 8B).

Time-lapse Analysis of Neuroblast Cell Division in Larval Brain Explants

Wild-type, $Lis1^{-}$, $Lis1^{-}$ $rod^{H4.8}$ (all 48 h ALH), or Gl^{1-3} (96 h ALH) late 2nd instar larvae (expressing either G147-GFP, His2AvD-GFP, or GFP-Rod under control of their native promoters) or *worniu-Gal4 UAS-GFP-Lis1* wandering 3rd instar larvae were dissected in D-22 (pH 6.75) insect medium (US Biological, Swampscott, MA) supplemented with 7.5% fetal bovine serum (FBS). Four to five larval brains were immediately transferred into 200 μl D-22 medium supplemented with 7.5% FBS, 0.5 mM ascorbic acid, and fatbodies obtained from 10 wild-type wandering 3rd instar larvae. Brains were mounted with fatbody tissue on a standard membrane (Yellow Springs Instruments, Yellow Springs, OH) and placed on a stainless steel slide as previously described (Kiehart *et al.*, 1994). Brains were imaged using a Bio-Rad Radiance 2000 laser scanning confocal microscope equipped with a 60× 1.4 NA oil immersion objective. For the analysis of spindle assembly (neuroblasts expressing 2 copies of G147-GFP), stacks containing four focal planes spaced by 1.5 μm were acquired at intervals of 10 s. For the analysis of chromosome movements and cell cycle timing (neuroblasts expressing one copy of His2AvD-GFP) or GFP-Rod localization, stacks containing six focal planes spaced by 1.5 μm were acquired at intervals of 15 s. For the analysis of GFP-Lis1 localization, stacks containing four focal planes spaced by 1.5 μm were acquired at intervals of 15 s. Time-lapse image series were converted into movies using MetaMorph (Universal Imaging, West Chester, PA) and ImageJ. All movie frames are maximum intensity projections.

Antibodies and Immunofluorescent Staining

Drosophila EST RE28987 was used to amplify a Lis1 cDNA encoding amino acids 1–90, which was subcloned into bacterial expression vectors to express 6xHis-tagged Lis1 protein. Purified 6xHis-Lis1 was injected into rats to generate polyclonal antibodies.

Larvae were dissected in Schneider's medium (Sigma, St. Louis, MO), fixed in 100 mM Pipes (pH 6.9), 1 mM EGTA, and 1 mM $MgCl_2$ for 25 min and blocked for 1 h in 1× phosphate-buffered saline (PBS) containing 1% bovine serum albumin and 0.1% Triton X-100 (PBS-BT). For labeling of DNA with propidium iodide, RNase A was added to a final concentration of 1 μg/ml. After blocking, specimen were extensively washed in PBS-BT for 1 h and incubated with primary antibodies in PBS-BT overnight at 4°C. Primary antibodies were: rat anti-Lis1 (1:2500; this study); rabbit anti-Gl (raised against Gl C-terminus, 1:150; Waterman-Storer and Holzbaur, 1996); rabbit anti-Cnn (1:1000; Heuer *et al.*, 1995); rabbit anti-nPKCζ (Santa Cruz Biotechnology, Santa Cruz, CA; 1:500); rat anti-Miranda (1:1000; Irion *et al.*, 2004); mouse anti-α-tubulin (DM1A, Sigma, 1:2000); rat anti-α-tubulin (MCA78S, Serotec, Raleigh, NC; 1:100); rabbit anti-Cid (1:500; Henikoff *et al.*, 2000); mouse anti-γ-tubulin (GTU-88, Sigma, 1:2000); rabbit anti-phospho-histone H3 (Upstate Biotechnology, Lake Placid, NY; 1:1000); rabbit anti-Rod (1:200; Scaerou *et al.*, 1999). Primary antibodies were extensively rinsed off with PBS-BT for 1 h at room temperature, and specimens were incubated with fluorescently conjugated secondary antibodies (Jackson ImmunoResearch Laboratories, West Grove, PA, and Molecular Probes, Eugene, OR) diluted in PBS-BT, followed by extensive rinsing with PBS-BT. For DNA labeling, specimens were mounted in FluoroGuard Antifade Reagent (Bio-Rad, Richmond, CA) containing 2.5 μg/ml propidium iodide. Brains were imaged using a Bio-Rad Radiance 2000 or Leica TCS SP2 laser scanning confocal microscope (Deerfield, IL) equipped with a 60× 1.4 NA or 63× 1.4 NA oil immersion objective, respectively. Figures were assembled in Adobe Photoshop (San Jose, CA).

Cell Cycle Analysis in Fixed Specimens

Larval brains were labeled for phospho-histone H3 (mitotic DNA), α-tubulin, and Miranda. Neuroblasts were identified by size and expression of Miranda protein, and scored for cell cycle stage using phospho-histone H3 and α-tubulin.

Immunoprecipitation Experiments

Immunoprecipitation experiments were conducted in high-speed supernatants at 4°C, and no microtubules were present. In detail, 0–24-h embryos were homogenized in 2.5 volumes IP buffer (50 mM HEPES, pH 7.2, 150 mM KCl, 0.9 M glycerol, 0.5 mM dithiothreitol, with protease inhibitors 10 μg/ml aprotinin, 1 μg/ml each leupeptin and pepstatin, 0.1 μg/ml each of soybean trypsin inhibitor, *n*-tosyl-L-arginine methylester, and benzamidine), and then supplemented with Triton X-100, 0.1%. After ultracentrifugation at 25,000 rpm for 20 min in a 50ti rotor, the supernatant was collected and precleared against washed protein A-Sepharose beads (Sigma). Cleared extract, 700 μl, was incubated 2 h at 4°C with beads that had previously been bound anti-Dhc monoclonal P1H4 (dynein heavy chain; McGrail and Hays, 1997), anti-GFP monoclonal 3E6 (Molecular Probes), or anti-Lis1 antibodies. Beads were washed in IP buffer three times, the last two washes without detergent. Pellets were eluted into 20 μl 2× sample buffer, and samples were analyzed by SDS-PAGE followed by Western analysis using anti-Dhc monoclonal P1H4 (McGrail and Hays, 1997); rabbit anti-Gl C-terminal (Waterman-Storer and Holzbaur, 1996) or anti-GFP monoclonal JL-8 (Clontech, Palo Alto, CA) antibodies.

Drug Treatments

Larval brains were dissected in Schneider's medium (Sigma) and incubated for 2 h at room temperature either in Schneider's medium supplemented with 30 μM colcemid (Sigma) or in Schneider's medium without drugs (controls). Afterward, brains were processed for immunofluorescent antibody staining as described above.

RESULTS

Time-lapse Analysis of the Cell Cycle in Larval Brain Neuroblasts

To determine a potential role of Lis1/Gl in mitotic checkpoint control, we sought to develop a time-lapse imaging method to visualize mitotic progression in living *Drosophila* neuroblasts of the intact larval brain. In a pioneering study, Savoian and Rieder (2002) described a live cell imaging technique to characterize key mitotic events in neuroblasts of wild-type larval brains squashed in Voltalef oil. Two major limitations of this method were that neuroblasts deteriorated relatively quickly in culture (within less than 2 h) and that wild-type neuroblasts contained secondary spindles besides the primary main spindle (in 17% of all observations) or failed to complete cytokinesis (Savoian and Rieder, 2002). Using a modified technique, Fleming and Rieder (2003) were able to prolong viability of neuroblasts in culture, but cytokinesis defects still occurred. We improved the original technique of Savoian and Rieder by making two essential changes: 1) minimizing physiological stress by substituting Voltalef oil with insect culture media, and 2) minimizing physical stress by imaging neuroblasts in whole larval brain explants instead of brain squashes (see *Materials and Methods*). Using this new technique, we never observed formation of secondary spindles or failure in cytokinesis in wild-type brains within the first 3 h of observation.

For our first set of experiments we imaged the GFP gene trap line *G147* (Morin *et al.*, 2001) that expresses an MT-associated GFP-fusion protein labeling spindle poles, spindle MTs, and astral MTs. Henceforth, we will refer to this GFP fusion protein as G147-GFP. The use of the *G147* line allowed us to precisely define many key stages of mitosis, including centrosome separation during prophase, initiation of prometaphase (defined by nuclear envelope breakdown [NEB] as judged by penetration of spindle microtubules into the cell center), and anaphase onset (defined by the first sign of widening of the gap between opposing kMTs). Here we used this time-lapse method to analyze the role of Lis1 in spindle assembly and mitotic checkpoint signaling.

Lis1 and Dynactin Are Required for Centrosome Separation and Spindle Assembly

Time-lapse imaging of wild-type second instar larval neuroblasts expressing G147-GFP showed that duplicated cen-

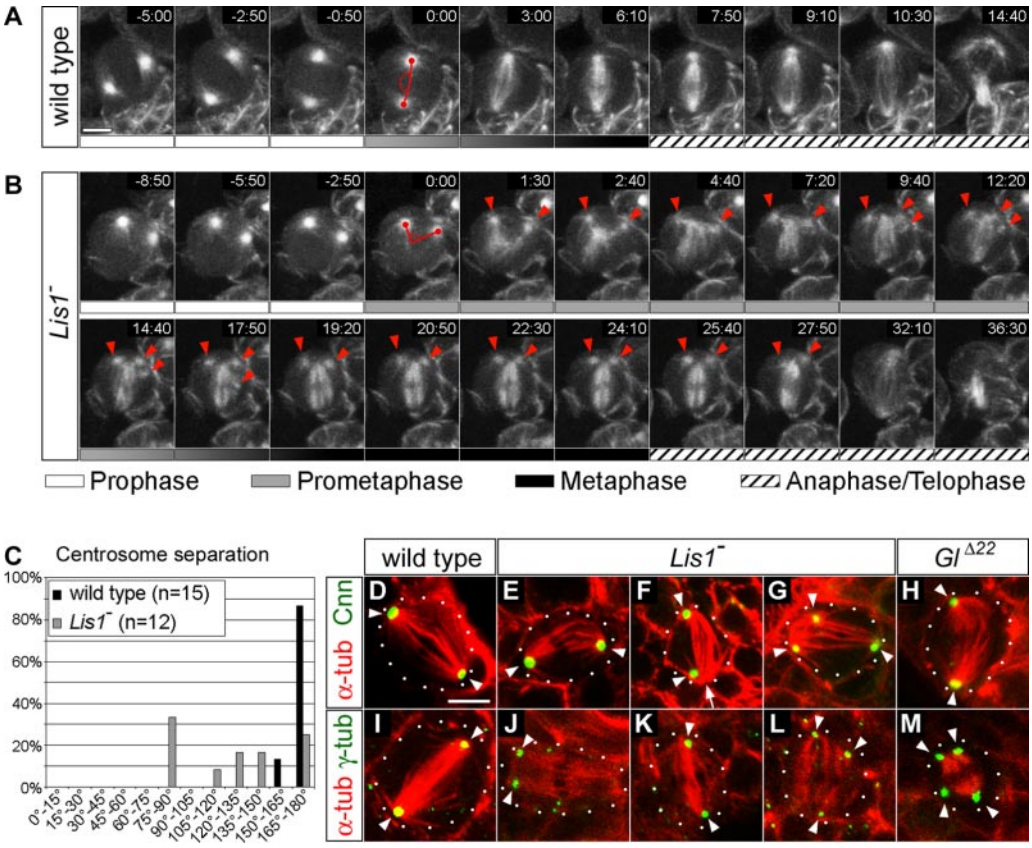

Figure 2. *Lis1* mutant neuroblasts exhibit defects in centrosome separation and spindle formation. (A and B) Dynamics of centrosome separation and spindle formation in larval neuroblasts expressing the G147-GFP MT-associated protein. In this and all subsequent figures, time is shown in min:sec relative to the onset of prometaphase (NEB, 0:00). Onset of prometaphase was determined as the moment the spindle microtubules penetrated into the cell center. Red lines indicate degree of centrosome separation calculated as the angle encompassed by two lines that were connected in the cell center and whose outer points were defined by the spindle poles at the time of prometaphase onset (0:00). Bars indicate cell cycle stages (see legend below B). (A) In wild-type neuroblasts, centrosomes were well separated and positioned on opposite sites of the nucleus at late prophase (−5:00). Centrosomes could rotate after this stage, but both remained positioned on opposite sides of the nucleus. After NEB (0:00), MTs formed a straight bipolar spindle (0:00–6:10; Supplementary Movie 1). (B) In *Lis1*$^{-}$ mutant neuroblasts, centrosome separation was frequently incomplete during prophase (−8:50–0:00). After NEB, MTs often had a wavy morphology and frequently assembled into a Y-shaped spindle (2:40). A central bipolar spindle generally formed after several minutes, although occasionally both MTOCs remained associated with the same spindle half (1:30–25:40, arrowheads). A few *Lis1*$^{-}$ neuroblasts contained more than two MTOCs, which usually reassociated with the spindle apparatus before cytokinesis (9:40–17:50, arrowheads; Supplementary Movie 2). (C) Quantification of centrosome separation defects in *Lis1*$^{-}$ mutant neuroblasts. (D–M) Wild-type, *Lis1*$^{-}$, and *Gl*$^{\Delta 22}$ mutant metaphase neuroblasts of 2nd instar larvae were double-labeled for α-tubulin and the centrosomal markers Centrosomin (Cnn; D–H) or γ-tubulin (I–M). Arrowheads indicate centrosomes. (D and I) Wild-type metaphase neuroblasts formed straight bipolar spindles with two centrosomes focusing MTs at the spindle poles. (E–H and J–M) *Lis1*$^{-}$ and *Gl*$^{\Delta 22}$ metaphase spindles exhibited various morphological defects, including curved spindles (E and H), one or two centrosomes unattached to spindle (F), two centrosomes on the same half spindle (J), or occasionally extra centrosomes (G, L, and M). Similar defects were observed in *Gl*$^{1-3}$/*Gl*$^{\Delta 22}$ mutant neuroblasts; see Table 1. *Lis1* and *Gl* mutant larval neuroblasts were on average smaller than wild-type counterparts. Bars, 5 μm.

trosomes stay in close proximity to each other until they separate during prophase. By the onset of prometaphase, the pair of centrosomes was always completely separated and positioned on opposite sides within the neuroblast (average separation 171 ± 7°, n = 15; Figure 2, A (0:00) and C, Supplementary Movie 1). As prometaphase progressed, the centrosomes nucleated MTs that formed a straight bipolar spindle (Figure 2A (0:00–6:10), Supplementary Movie 1).

To investigate the role of Lis1 in centrosome separation and spindle formation, we performed a similar time-lapse analysis on 2nd instar larval neuroblasts transheterozygous for two previously described *Lis1* alleles, *Lis1*$^{G10.14}$ and *Lis1*^{k13209} (Liu *et al.*, 1999). In *Lis1*$^{G10.14}$/*Lis1*^{k13209} (hereafter referred to as *Lis1*$^{-}$) larval brains, Lis1 protein was reduced below detectable levels (see below and Figure 9). In contrast to wild-type, time-lapse imaging of *Lis1*$^{-}$ mutant neuroblasts expressing G147-GFP revealed that centrosome separation was frequently incomplete at the onset of prometaphase (average separation 124 ± 38°, n = 12; Figure 2, B (0:00) and C, Supplementary Movie 2), and MTs emanating from both spindle poles often developed a Y-shaped morphology during prometaphase, presumably because of the close apposition of the centrosomes (Figure 2B (0:00–2:40), Supplementary Movie 2). Strikingly, these Y-shaped spindles generally "recovered" to form seemingly bipolar arrays of kMTs by late metaphase (Figure 2B (17:50–24:10), Supplementary Movie 2). However, despite the apparent bipolar spindle organization, microtubule organizing centers (MTOCs) occasionally detached from spindles or two

Table 1. Spindle morphology and centrosome number

	Wild type[a] (n = 53)	*Lis1*$^{-}$ (n = 105)	$Gl^{1-3}/Gl^{\Delta 22}$ (n = 89)	$Gl^{\Delta 22}$ (n = 140)
Spindle morphology[b]				
Bipolar, straight	92.5%	50.2%	63.6%	73.1%
Bipolar, curved	5.6%	17.7%	9.1%	11.9%
Bipolar, spindle pole(s) unfocused	1.9%	12.9%	12.5%	7.5%
Bipolar, centrosome(s) unattached	0.0%	8.6%	4.6%	2.2%
Bipolar, 2 centrosomes on half-spindle	0.0%	1.0%	3.4%	1.5%
No bipolar MT organization	0.0%	11.0%	6.8%	3.7%
Centrosome number[c]				
2	100.0%	95.2%	93.6%	95.7%
3–4	0.0%	4.8%	6.4%	4.3%

[a] Genotypes: wild type (*y w*); *Lis1*$^{-}$ ($Lis1^{G10.14}/Lis1^{k13209}$); $Gl^{1-3}/Gl^{\Delta 22}$; $Gl^{\Delta 22}$ ($Gl^{\Delta 22}/Gl^{\Delta 22}$).

[b] Only cells that contained 2 centrosomes were considered.

[c] The number of centrosomes based on number of distinct Cnn/γ-Tubulin protein foci.

MTOCs appeared to maintain attachment to the same side of a half-spindle. In few cases neuroblasts contained more than the normal two MTOCs (Figure 2B (17:50–24:10), Supplementary Movie 2). We conclude that Lis1 is required for centrosome separation, proper spindle assembly, and regulation of MTOC number.

To analyze spindle formation defects at higher spatial resolution and to determine the nature of the observed supernumerary MTOCs, we assayed centrosome (Centrosomin and γ-tubulin) and spindle markers (α-tubulin) in fixed neuroblasts. We found that wild-type metaphase neuroblasts had a straight bipolar spindle with each spindle pole tightly focused on a single centrosome (Figure 2, D and I, Table 1). In contrast, *Lis1*$^{-}$ mutant neuroblasts showed curved spindles, unfocused spindle poles, spindles with one or two unattached centrosomes, or even spindles in which both centrosomes were attached to the same half-spindle (Figure 2, E, F, J, and K; Table 1). Strikingly, some of these metaphase neuroblasts appeared to contain 3–4 centrosomes with multipolar spindles, bipolar spindles with more than one centrosome on each half spindle, or bipolar spindles with 1–2 unattached centrosomes (Figure 2, G and L, Table 1). Because of the lack of suitable *Drosophila* centriole markers, we were unable to determine whether all ectopic centrosomelike (Centrosomin/γ-tubulin positive) structures contained centrioles. We conclude that Lis1 has a critical role in correct spindle assembly by regulating centrosome separation, focusing of spindle poles, centrosome attachment, and centrosome number and/or centrosome integrity in larval neuroblasts. The presence of a subset of *Lis1*$^{-}$ mutant neuroblasts with normal bipolar spindles, however, allowed us to examine these neuroblasts for defects in later steps of the cell cycle (see next section).

Lis1 functions together with dynactin in many cell types, so we wanted to determine if dynactin was also required for spindle formation. Well-characterized loss-of-function dynactin mutants do not exist in *Drosophila*, so we generated a null mutation in *Glued* ($Gl^{\Delta 22}$), which encodes the largest dynactin subunit, as well as molecularly characterized an extant allele, Gl^{1-3} (Harte and Kankel, 1982; Figure 1; see *Materials and Methods*). Both $Gl^{\Delta 22}$ and Gl^{1-3} appeared to comprise protein-null alleles (see below, Figure 9). We found that $Gl^{\Delta 22}$ homozygous or Gl^{1-3} hemizygous mutant neuroblasts phenocopied centrosome and spindle formation defects observed in *Lis1*$^{-}$ mutants. Defects included metaphase neuroblasts with curved spindles, unfocused spindle poles, spindles with one or two unattached centrosomes, spindles in which both centrosomes were attached to the same half-spindle, or occasionally neuroblasts with three or four centrosomes forming bipolar or multipolar spindles (Figure 2, H and M, Table 1, and unpublished data). Thus, both dynactin and Lis1 promote centrosome separation and proper spindle formation in larval *Drosophila* neuroblasts.

Lis1 and Dynactin Are Required for Timely Anaphase Onset

In wild-type neuroblasts (expressing *G147-GFP*), the duration of prometaphase and metaphase (from NEB to anaphase onset) was quite rapid and highly reproducible, lasting 6 min 12 s ± 0 min 49 s (n = 18; Figure 3, A and D, Supplementary Movie 1). In contrast, *Lis1*$^{-}$ mutant neuroblasts showed dramatic lengthening of the prometaphase/metaphase interval to an average of 46 min 54 s ± 18 min 33 s (n = 11, Figure 3, B and D, Supplementary Movie 3). We reasoned that this delay in anaphase onset might be due to extended mitotic checkpoint activity. To test this, we reduced Rod function to bypass the checkpoint (Basto *et al.*, 2000). In *Lis1*$^{-}$ $rod^{H4.8}$ double mutant neuroblasts, progression through prometaphase/metaphase only took 11 min 31 s ± 4 min 23 s (n = 11, Figure 3, C and D, Supplementary Movie 4), confirming that the delay in anaphase onset is checkpoint-dependent. Note that centrosome separation and spindle assembly defects were still present in *Lis1*$^{-}$ $rod^{H4.8}$ double mutant neuroblasts, indicating that these defects were independent of altered mitotic checkpoint signaling (Figure 3C, Supplementary Movie 4, and unpublished data). In addition, we also calculated mitotic index and metaphase:anaphase ratio in fixed specimens of wild type, *Gl* single, *Lis1*$^{-}$ single, and *Lis1*$^{-}$ $rod^{H4.8}$ double mutants. Both mitotic index and metaphase:anaphase ratio of neuroblasts were increased in *Lis1*$^{-}$ and *Gl* single mutants compared with wild-type and *Lis1*$^{-}$ $rod^{H4.8}$ double mutant neuroblasts (Table 2). Thus, the observed delays in anaphase onset in *Lis1* and *Gl* mutant neuroblasts are consistent with extended mitotic checkpoint activity, indicating a role for Lis1/dynactin in satisfying or inactivating the mitotic checkpoint.

To measure the length of prometaphase and metaphase individually, we expressed a single copy of a GFP-tagged histone variant His2AvD under control of its native promoter (His2AvD-GFP; Clarkson and Saint, 1999) in larval neuroblasts. We defined prometaphase as the interval from NEB (evident by a slight increase of cytoplasmic His2AvD-

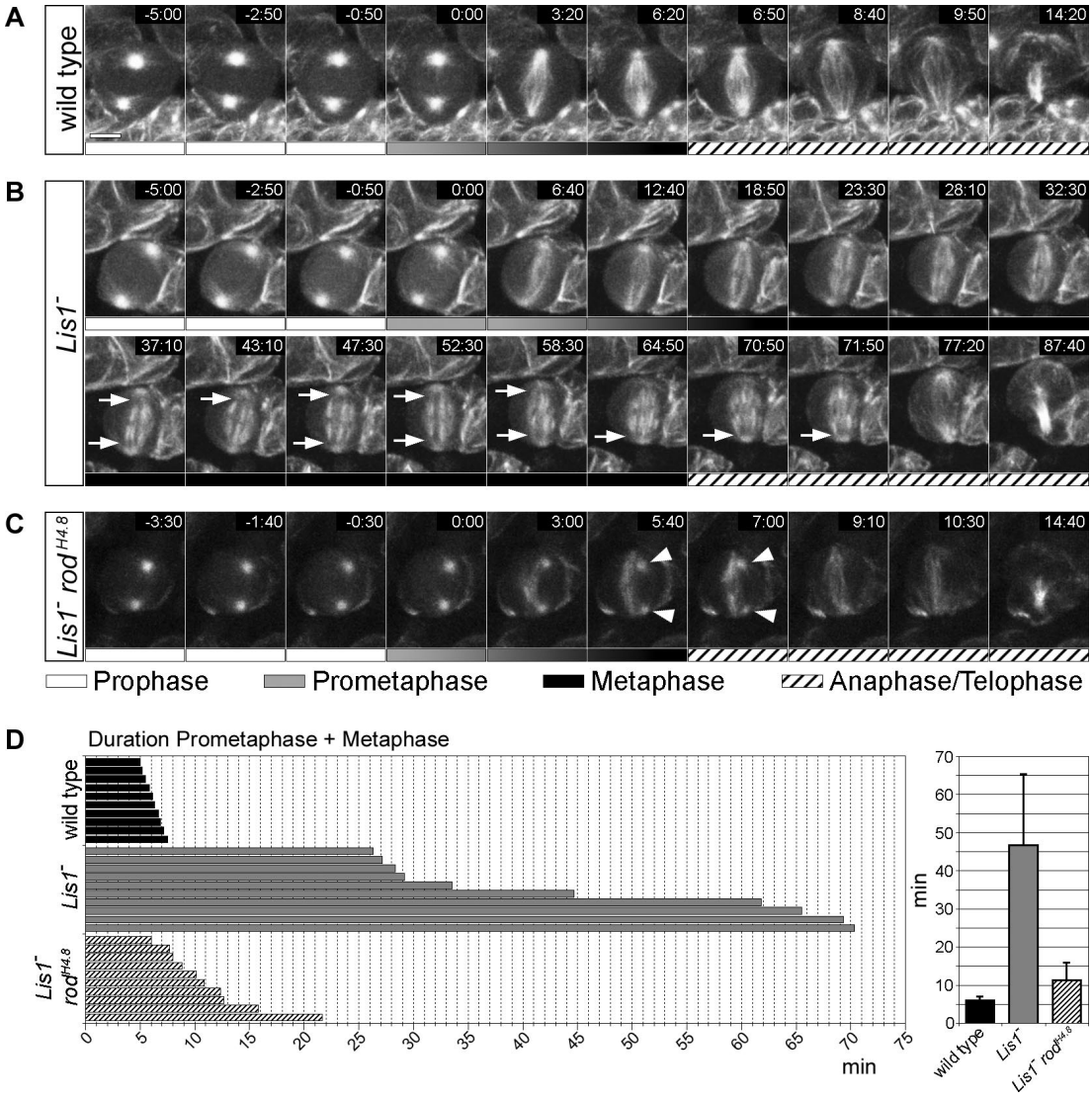

Figure 3. *Lis1* mutant neuroblasts exhibit mitotic checkpoint-dependent delays in anaphase onset. Cell cycle timing was determined in larval neuroblasts expressing the G147-GFP MT-associated protein. Bars indicate cell cycle stages (see legend below C). (A) In wild-type neuroblasts, prometaphase and metaphase took 5–8 min (similar to Supplementary Movie 1). (B) In *Lis1*$^{-}$ mutant neuroblasts, prometaphase/metaphase took 27–71 min (Supplementary Movie 3). Arrows indicate apparent detachment of kMTs from MTOCs. (C) In *Lis1*$^{-}$ *rod*$^{H4.8}$ double mutant neuroblasts, prometaphase/metaphase took 6–22 min (Supplementary Movie 4). Note that spindle assembly was still defective and MTOCs could detach from the spindle apparatus (arrowheads). The GFP signal appears dimmer (compared with signal of neuroblasts depicted in A and B) because the neuroblast was positioned deeper in the brain. All neuroblasts were imaged using identical laser settings. Bar, 5 μm. (D) Quantification of prometaphase/metaphase duration in wild-type, *Lis1*$^{-}$ single mutant, and *Lis1*$^{-}$ *rod*$^{H4.8}$ double mutant neuroblasts. The left histogram depicts duration of prometaphase/metaphase for 10 neuroblasts of each genotype (including neuroblasts with shortest and longest prometaphase/metaphase as well as 8 randomly chosen neuroblasts for each genotype). The right histogram depicts the calculated mean duration of prometaphase/metaphase + SD for each genotype (wild type (n = 18), *Lis1*$^{-}$ (n = 11), *Lis1*$^{-}$ *rod*$^{H4.8}$ (n = 11)).

GFP fluorescence intensity not associated with chromosomes) to the moment of completed chromosome congression on the metaphase plate, and we defined metaphase as the interval between completion of chromosome congression and initiation of poleward chromosome movement. In wild-type neuroblasts, prometaphase and metaphase took 4 min 14 s ± 1 min 31 s and 2 min 24 s ± 1 min 13 s, respectively (n = 12, Figure 4, A and D, Supplementary Movie 5). Throughout metaphase, all chromosomes remained aligned in a tight metaphase plate. In contrast, in *Lis1*$^{-}$ mutant neuroblasts both prometaphase (mean duration 32 min 18 s ± 15 min 55 s) and metaphase (mean duration 19 min 21 s ± 16 min 35 s) were significantly prolonged (n = 10, Figure 4, B–D, Supplementary Movies 6 and 7). These data indicate that Lis1/Gl affects cell cycle timing in at least two ways. First, Lis1/Gl is required for timely prometaphase progression, possibly by promoting spindle assembly and thereby facilitating efficient MT-kinetochore capturing/chromosome congression. Second, Lis1/Gl is also required for the timely initiation of the metaphase-to-anaphase transition, possibly by contributing to mitotic checkpoint inactivation.

Table 2. Cell cycle profile in larval neuroblasts

	Wild type (n = 428)[a]	*Lis1*$^{-}$ (n = 294)	*Lis1*$^{-}$ *rod* $^{H4.8}$ (n = 446)	*rod* $^{H4.8}$ (n = 356)	*Gl* $^{1-3}$/*Df* (n = 429)	*Gl* $^{\Delta 22}$ (n = 346)
Cell cycle profile[b]						
Interphase	75.1%	42.2%	78.3%	69.4%	66.7%	68.5%
Prophase	11.9%	13.6%	8.5%	14.0%	14.3%	11.2%
Prometa-/Metaphase	6.9%	41.5%	6.5%	7.6%	17.6%	18.5%
Anaphase	1.4%	1.0%	2.0%	2.3%	0.7%	1.2%
Telophase	4.7%	1.7%	4.7%	6.7%	0.7%	0.6%
Mitotic index[c]	24.9%	57.8%	21.7%	30.6%	33.3%	31.5%
Metaphase:anaphase[d]	4.9	41.5	3.3	3.4	25.0	15.4

[a] Genotypes: wild type (*y w*); *Lis1*$^{-}$ (*Lis1*$^{G10.14}$/*Lis1*^{k13209}); *Lis1*$^{-}$ *rod*$^{H4.8}$ (*Lis1*$^{G10.14}$/*Lis1*^{k13209} *rod*$^{H4.8}$/*rod*$^{H4.8}$); *rod*$^{H4.8}$ (*rod*$^{H4.8}$/*rod*$^{H4.8}$); *Gl*$^{1-3}$/*Df* (*Gl*$^{1-3}$/*Df(3L)fz-Gf3b*); *Gl*$^{\Delta 22}$ (*Gl*$^{\Delta 22}$/*Gl*$^{\Delta 22}$).

[b] The percentile of neuroblasts at given cell cycle stage.

[c] The percentile of mitotic neuroblasts relative to total number of neuroblasts.

[d] The number of metaphase divided by the number of anaphase neuroblasts.

Lis1 and Gl Are Required to Transport Checkpoint Proteins from Kinetochores and Generate Interkinetochore Tension

Loss of Lis1/dynactin function could cause prolonged mitotic checkpoint activity by several mechanisms, including impairment of MT-kinetochore attachment (Rieder *et al.*, 1995), a reduction of interkinetochore tension (Li and Nicklas, 1995), or a defect in the transport of checkpoint proteins off kinetochores (Howell *et al.*, 2001; Wojcik *et al.*, 2001). Here we tested which, if any, of these mechanisms were affected in *Lis1* and *Gl* mutant neuroblasts.

We first tested whether defective MT-kinetochore attachment was the primary cause of delayed metaphase-to-anaphase transition in *Lis1* and *Gl* mutant neuroblasts. Analysis of fixed preparations stained for spindle, DNA, and/or kinetochore markers revealed that in *Lis1* and *Gl* single mutant metaphase neuroblasts typically all chromosomes had congressed into a tight metaphase plate with kinetochore fibers abutting kinetochores (*Lis1*$^{-}$: 72.5%, n = 102; *Gl*$^{1-3}$: 75.0%, n = 40; *Gl*$^{1-3}$/*Df(3L)fz-GF3b*: 69.2%, n = 107; Figure 5, C and D). In addition, we followed chromosome movement (visualized with His2AvD-GFP) in *Lis1*$^{-}$ mutant neuroblasts using time-lapse analysis. We found that during prometaphase chromosomes showed delayed congression to the equatorial plate but eventually aligned into a tight metaphase plate (Figure 4, B and C, Supplementary Movies 6 and 7, n = 10). In two *Lis1*$^{-}$ mutant neuroblasts, we observed formation of a tight metaphase plate, subsequent chromosome loss, and recongression of the lost chromosome to the metaphase plate (Figure 4C (17:15–40:45), Supplementary Movie 7). Importantly, even after congression of all chromosomes into a tight metaphase plate, *Lis1*$^{-}$ mutant metaphase neuroblasts showed delayed transition into anaphase (Figure 4B (25:15–33:15) and 4C (40:45–45:30), Supplementary Movies 6 and 7). Although chromosome separation in *Lis1*$^{-}$ mutant anaphase neuroblasts was slightly slower than in wild-type counterparts, chromosomes were always completely partitioned in both daughter cells in these mutants (n = 10). We conclude that defective MT-kinetochore attachment is unlikely to be the only cause of extended checkpoint activity in *Lis1* (and *Gl*) mutant neuroblasts.

We next analyzed whether *Lis1* or *Gl* mutants showed loss of interkinetochore tension. Kinetochores assemble on specific DNA regions called centromeres. Centromeric nucleosomes contain a histone H3-like protein, named CENP-A or Cid (Centromere Identifier) in flies (Henikoff *et al.*, 2000). Increased tension between sister kinetochores is evident by increased distance between sister centromeres (intercentromere distance). During prophase, in the absence of MT-kinetochore attachment, the measured intercentromere distance reflects the "resting length" corresponding to 0% tension. We found that wild-type, *Lis1* mutant, and *Gl* mutant prophase neuroblasts showed statistically indistinguishable intercentromere resting lengths (wild type: 0.51 ± 0.08 μm, n = 36; *Lis1*$^{-}$: 0.51 ± 0.07 μm, n = 20; *Gl*$^{1-3}$: 0.55 ± 0.07 μm, n = 5; Student's *t* test analysis revealed p values > 0.2 in all pair wise combinations, Figure 5, A and E). On entry into metaphase, the wild-type intercentromere length increased to 1.10 ± 0.13 μm (n = 36, Figure 5, B and E), which presumably reflects 100% tension. In *Lis1* and *Gl* mutant metaphase neuroblasts the intercentromere distance was slightly but significantly reduced compared with wild-type metaphase counterparts (*Lis1*$^{-}$: 0.97 ± 0.16 μm, n = 58; *Gl*$^{1-3}$: 0.93 ± 0.13 μm, n = 25; p < 0.001; Figure 5, C–E). Assuming a linear correlation between measured intercentromere distance and generated tension, we calculated that tension was reduced to ~77 and ~70% in *Lis1* and *Gl* mutant metaphase neuroblasts, respectively. Thus, it is possible that the observed reduction in interkinetochore tension activates the mitotic checkpoint and delays anaphase onset in *Lis1* and *Gl* mutant neuroblasts (see *Discussion*).

To test whether checkpoint protein localization was normal in *Lis1* and *Gl* mutant neuroblasts, we assayed the dynamic localization of GFP-Rod. GFP-Rod was expressed under the control of the native Rod promoter in a *rod* mutant background (Scaerou *et al.*, 1999; Basto *et al.*, 2004). In wild-type neuroblasts, GFP-Rod was excluded from the nucleus during interphase and prophase, but accumulated on unattached kinetochores at the onset of prometaphase (Figure 6A (0:00), Supplementary Movie 8). At metaphase, GFP-Rod moved from kinetochores onto kMTs (Figure 6A (2:15–5:30), Supplementary Movie 8), presumably as a result of poleward streaming along kMTs (Basto *et al.*, 2004). In contrast, *Lis1*$^{-}$ mutant neuroblasts lacked poleward GFP-Rod streaming and thus showed persistent GFP-Rod kinetochore localization during metaphase and anaphase (Figure 6B (0:00–49:15), Supplementary Movie 9). In addition, we confirmed that GFP-Rod resembled endogenous Rod localization by analyzing fixed preparations. In wild-type neuroblasts,

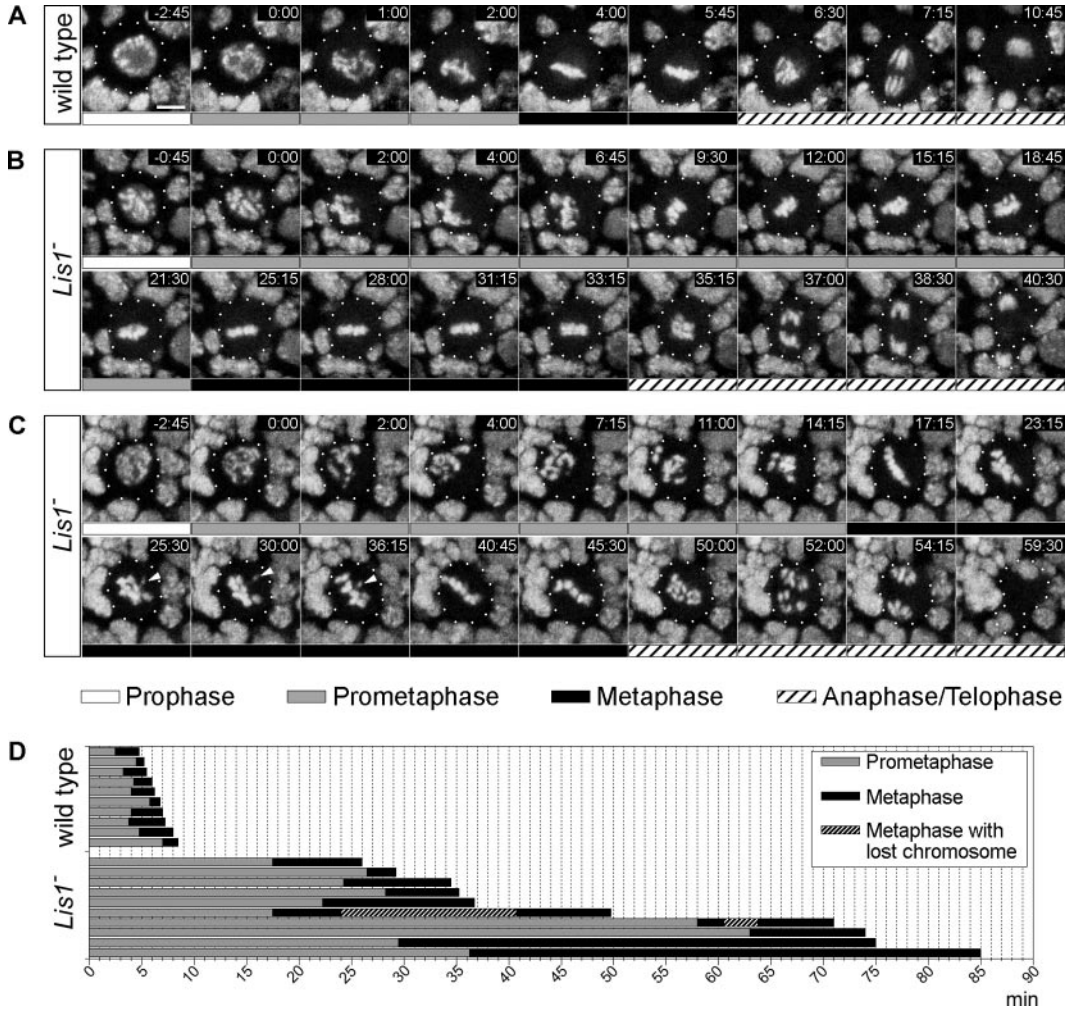

Figure 4. *Lis1* mutant neuroblasts show delayed chromosome congression to the metaphase plate and prolonged metaphase. Chromosome movement and cell cycle timing was assayed in larval neuroblasts expressing GFP-tagged His2AvD protein. Bars indicate cell cycle stages (see legend below C). (A) In wild-type neuroblasts, chromosomes completed congression into a tight metaphase plate within 2–7 min after NEB (Supplementary Movie 5). These neuroblasts stayed in metaphase for 2–4 min. (B and C) In *Lis1*$^-$ mutant neuroblasts, chromosome congression was severely delayed and prometaphase took 17–63 min (Supplementary Movies 6 and 7). Metaphase was also prolonged and took 3–49 min. In two neuroblasts we observed chromosomes that were lost from and recongressed to the metaphase plate (C, 25:30–36:15, arrowheads, Supplementary Movie 7). Bar, 5 μm. (D) Quantification of prometaphase and metaphase duration in wild-type and *Lis1*$^-$ mutant neuroblasts. Depicted are durations of prometaphase and metaphase for 10 neuroblasts of each genotype (for wild type including neuroblasts with shortest and longest prometaphase/metaphase interval as well as 8 randomly chosen neuroblasts).

Rod localized to prometaphase kinetochores and redistributed along kMTs during metaphase (Figure 7, B and C). In *Lis1*, *Gl,* and *dhc* (*dynein heavy chain*) mutant neuroblasts we observed persistent high level of Rod localization at metaphase kinetochores that were seemingly attached to MTs (Figure 7, D–F), consistent with the notion that a Lis1/dynactin/dynein complex is required for timely removal of the Rod checkpoint protein from kinetochores at metaphase.

Lis1 and Dynactin Coimmunoprecipitate with Dynein and Colocalize with the Checkpoint Protein Rod on Kinetochores

We have shown that Lis1 and dynactin have similar functions throughout the cell cycle, ranging from centrosome separation to generation of interkinetochore tension and checkpoint protein transport. We next determined whether Lis1/dynactin are physically associated in vivo, and we analyzed subcellular localization of Lis1/dynactin throughout the neuroblast cell cycle. Using anti-Lis1 antibodies, we could immunoprecipitate both dynein and dynactin subunits, and in a reciprocal experiment we used anti-Dhc antibodies to immunoprecipitate Gl protein (Figure 8A). We also expressed full-length Lis1 protein fused to GFP (GFP-Lis1) in wild-type embryos and showed it could immunoprecipitate Dhc and Gl proteins; similarly, both anti-Dhc and anti-Gl antibodies could immunoprecipitate GFP-Lis1 (Figure 8B and unpublished data). From these results we conclude that some Lis1, dynactin, and dynein proteins are associated in a complex in *Drosophila* embryos. However, our immunoprecipitations were not quantitative, and we did not determine the percentage of each protein that exists together in a complex. Our findings support previous observations reported for the interaction of dynein, Lis1, and dynactin in mammalian brain cytosolic extracts (Faulkner *et al.*, 2000; Smith *et al.*, 2000).

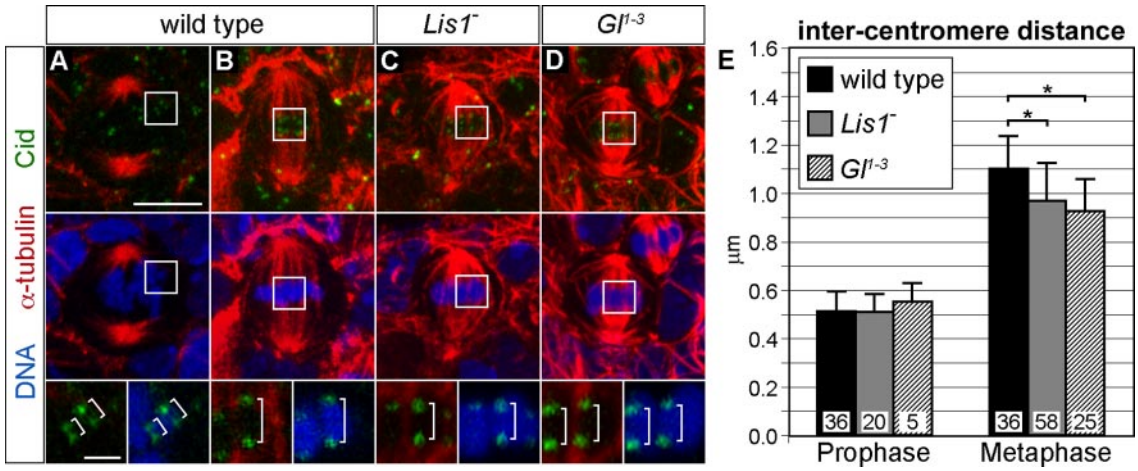

Figure 5. Tension between sister centromeres is reduced in *Lis1* and *Gl* mutant metaphase neuroblasts. Wild-type (A, B), *Lis1*$^{-}$ (C), and *Gl*$^{1-3}$ (D) mutant neuroblasts were triple labeled for α-tubulin, Cid (centromeres), and DNA. Top and middle rows show maximum intensity projections of three-dimensional image stacks containing 10–20 0.2-μm sections. Squares indicate regions shown at higher magnification in bottom row. Bottom row shows individual sister centromere pairs in single focal planes at high magnification. Brackets indicate sister centromere pairs. (A) In wild-type prophase neuroblasts, centromere pairs were closely apposed due to the absence of MT attachment and tension. (B) In wild-type metaphase neuroblasts, centromere pairs were aligned at the equatorial plate. Because of MT attachment and generation of tension on kinetochores, the distance between sister centromeres was increased. (C and D) In *Lis1*$^{-}$ (C) and *Gl*$^{1-3}$ (D) mutant metaphase neuroblasts, distance between sister centromeres was slightly smaller than its wild-type metaphase counterparts, but still significantly larger than between wild-type prophase sister centromeres. (E) Quantification of measured distances between sister centromeres in prophase and metaphase neuroblasts of the indicated genotypes. Depicted are means + SDs. Student's *t* test analysis revealed no significant difference in sister centromere distance in wild-type, *Lis1*$^{-}$, and *Gl*$^{1-3}$ mutant prophase neuroblasts ($p > 0.2$ in all pairwise combinations). Sister centromere distance was slightly but significantly reduced in *Lis1*$^{-}$ and *Gl*$^{1-3}$ mutant metaphase neuroblasts compared with wild-type counterparts ($p < 0.001$, indicated by brackets and asterisks). No statistically significant difference in sister centromere distance was observed in *Lis1*$^{-}$ and *Gl*$^{1-3}$ mutant neuroblasts ($p > 0.1$). Numbers of analyzed centromere pairs are depicted at the bottom of each histogram bar. Bars, 5 μm in top and middle rows, 1 μm in bottom row.

We next assayed the subcellular localization of Lis1 and Gl proteins in mitotic neuroblasts. Lis1 and Gl showed spindle pole/centrosome association from late prophase through telophase (Figure 9, A-B and F-G, and unpublished data). Both proteins were colocalized with Rod on prometaphase kinetochores (Figure 7B and unpublished data), and distributed along kMTs during metaphase (Figures 7C and 9, B and G). During anaphase/telophase, Lis1/dynactin staining intensity was diminished on kMTs (unpublished data). A similar localization at centrosomes and kinetochores has been reported for dynein (Pfarr *et al.*, 1990; Steuer *et al.*, 1990; Starr *et al.*, 1998; Gonczy *et al.*, 1999; Wojcik *et al.*, 2001). In *Lis1* and

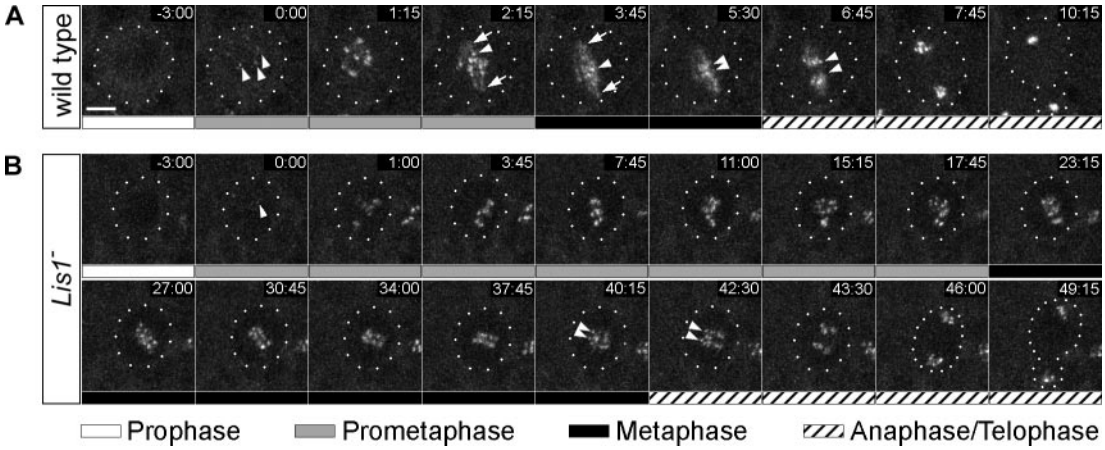

Figure 6. Dynamics of Rod localization in wild-type and *Lis1* mutant neuroblasts. GFP-Rod protein was expressed in wild-type (A) and *Lis1*$^{-}$ mutant (B) larval neuroblasts. Dotted circles indicate neuroblast outlines. Bars indicate cell cycle stages (see legend below B). (A) In wild-type interphase neuroblasts, GFP-Rod was weakly detectable in the cytoplasm, but not in the nucleus (−3:00). During prometaphase, GFP-Rod accumulated on unattached kinetochores shortly after NEB (0:00–1:15, arrowheads), and was detectable along spindle fibers (arrows) during prometaphase (2:15) and metaphase (3:45–5:30). During anaphase GFP-Rod gradually disappeared from spindle kMTs, but was still detectable on kinetochores (6:45–7:45; Supplementary Movie 8). (B) In *Lis1*$^{-}$ mutant neuroblasts, GFP-Rod was detectable on kinetochores during prometaphase (0:00–17:45), but failed to redistribute along spindle MTs during metaphase (23:15–40:15). GFP-Rod protein remained localized to kinetochores during anaphase/telophase (42:30–49:15; Supplementary Movie 9). Bar, 5 μm.

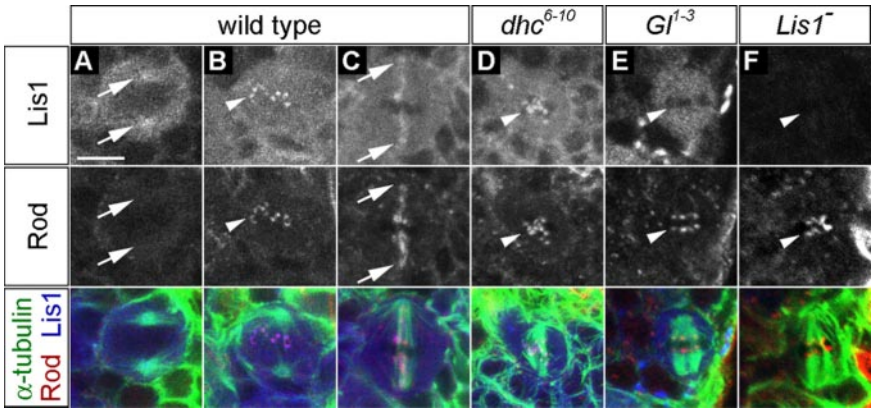

Figure 7. Rod protein transport off kinetochores is impaired in *Lis1*, *Gl*, and *dhc* mutant neuroblasts. Wild type (A–C), dhc^{6-10} (D), Gl^{1-3} (E), and $Lis1^{-}$ (F) mutant neuroblasts were triple-labeled for Lis1 (top row), Rod (middle row), and α-tubulin. Merged images are shown in bottom row. Arrows and arrowheads indicate spindle poles and kinetochores, respectively. (A) Wild-type prophase neuroblast with Lis1 but not Rod on centrosomes. (B) Wild-type prometaphase neuroblast showing colocalization of Lis1 and Rod on kinetochores. (C) Wild-type metaphase neuroblast showing Lis1 and Rod codistributed along spindle MTs. (D) dhc^{6-10} mutant late prometaphase/early metaphase neuroblast showing colocalization of Lis1 and Rod protein on kinetochores. (E) Gl^{1-3} mutant metaphase neuroblast with Rod localization on kinetochores. Lis1 protein is not detectable on kinetochores above cytoplasmic levels. (F) $Lis1^{-}$ mutant metaphase neuroblasts with Rod localization on kinetochores. Bar, 5 μm.

Gl mutant neuroblasts, Lis1 and Gl proteins were undetectable at all of these locations, respectively, demonstrating that labeling of these structures with the anti-Lis1 and anti-Gl antibodies was specific (Figure 9, D, J, and K). Furthermore, we observed the same localization of a GFP-tagged full-length Lis1 (GFP-Lis1) protein in live neuroblasts. In prophase neuroblasts, GFP-Lis1 was excluded from the nucleus. With the beginning of prometaphase GFP-Lis1 was strongly associated with kinetochores. During late prometaphase/metaphase, GFP-Lis1 made a transition from kinetochore to centrosomal/spindle localization, whereas during anaphase and telophase there was progressively less GFP-Lis1 associated with the mitotic spindle (Figure 10A, Supplementary Movie 10).

In summary, Lis1/dynactin/dynein coimmunoprecipitate, localize to centrosome/spindle poles, and are transiently colocalized with the checkpoint protein Rod on prometaphase kinetochores before enrichment on kMTs. These results are consistent with a function of Lis1/dynactin/dynein in centrosome separation and spindle assembly as well as kinetochore-based checkpoint function (see *Discussion*).

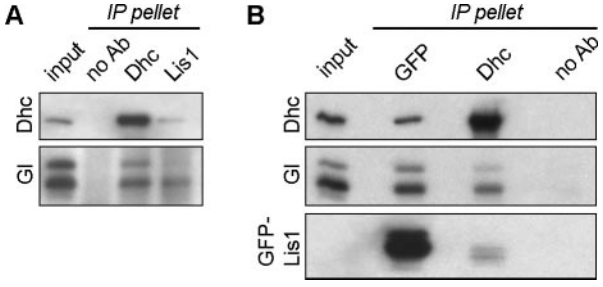

Figure 8. Lis1 coimmunoprecipitates with dynactin and cytoplasmic dynein subunits. (A) Immunoprecipitation of Dhc (top row) and Gl (bottom row) proteins from wild-type embryonic lysates with anti-Dhc and anti-Lis1 antibodies (lanes 3 and 4, respectively). The reduced amount of the upper Gl polypeptide in lane 4 accompanies some degradation of the sample and is not the result of selective precipitation of a single Glued polypeptide (see also B, lane 2). (B) Immunoprecipitation of Dhc (top row), Gl (middle row), and GFP-Lis1 (bottom row) protein from lysates of transgenic embryos expressing a GFP-Lis1 fusion protein using anti-GFP and anti-Dhc antibodies (lanes 2 and 3, respectively).

Lis1 and Dynactin Are Codependent for Kinetochore Localization

Lis1/dynactin localization to kinetochores is evolutionarily conserved, but appears to be regulated differently in mammalian and *C. elegans* cell types (Coquelle *et al.*, 2002; Tai *et al.*, 2002; Cockell *et al.*, 2004). Here we investigated the interdependence of Lis1 and dynactin kinetochore localization in *Drosophila* neuroblasts. We found that after reduction of dynein activity (in dhc^{6-10} mutants, Gepner *et al.*, 1996; Wojcik *et al.*, 2001), the initial localization of Lis1, dynactin, and the mutant Dhc^{6-10} proteins (Wojcik *et al.*, 2001) to kinetochores was normal, but Lis1/dynactin failed to become depleted from metaphase kinetochores (Figure 9, C and H). Thus, dynein activity is required for transporting Lis1 and dynactin off the kinetochore along kMTs. In contrast, *Lis1* mutant neuroblasts lacked Gl kinetochore localization (Figure 9I), and *Gl* mutant neuroblasts lacked Lis1 kinetochore localization (Figures 7E and 9E). This was true even when microtubules were depolymerized to block potential dynein-based transport off kinetochores, strongly suggesting that in *Drosophila* neuroblasts Lis1 and Gl are codependent for kinetochore localization.

DISCUSSION

Lis1/Dynactin Regulate Centrosome Separation and Spindle Assembly

We showed that both Lis1 and Gl are enriched on centrosomes/spindle poles in wild-type neuroblasts and that Lis1/Gl are required for centrosome separation in prophase neuroblasts. A role for centrosome separation has previously been reported for dynein in *Drosophila* embryos, dynein in mammalian cells, and dynein/dynactin/Lis1 in *C. elegans* blastomeres (Vaisberg *et al.*, 1993; Gonczy *et al.*, 1999; Robinson *et al.*, 1999; Cockell *et al.*, 2004; Schmidt *et al.*, 2005). However, the exact mechanism by which they promote centrosome separation is unclear. One proposed model suggests that dynein may promote centrosome separation by generating pulling forces on astral MTs attached to the cortex or cytoplasmic structures (Vaisberg *et al.*, 1993; Waters *et al.*, 1993). Alternatively, dynein associated with the nuclear envelope may exert pulling forces on astral MTs to promote centrosome separation (Gonczy *et al.*, 1999; Robinson *et al.*, 1999). We did not detect GFP-Lis1 on the nuclear envelope or at the neuroblast cortex, although it is possible

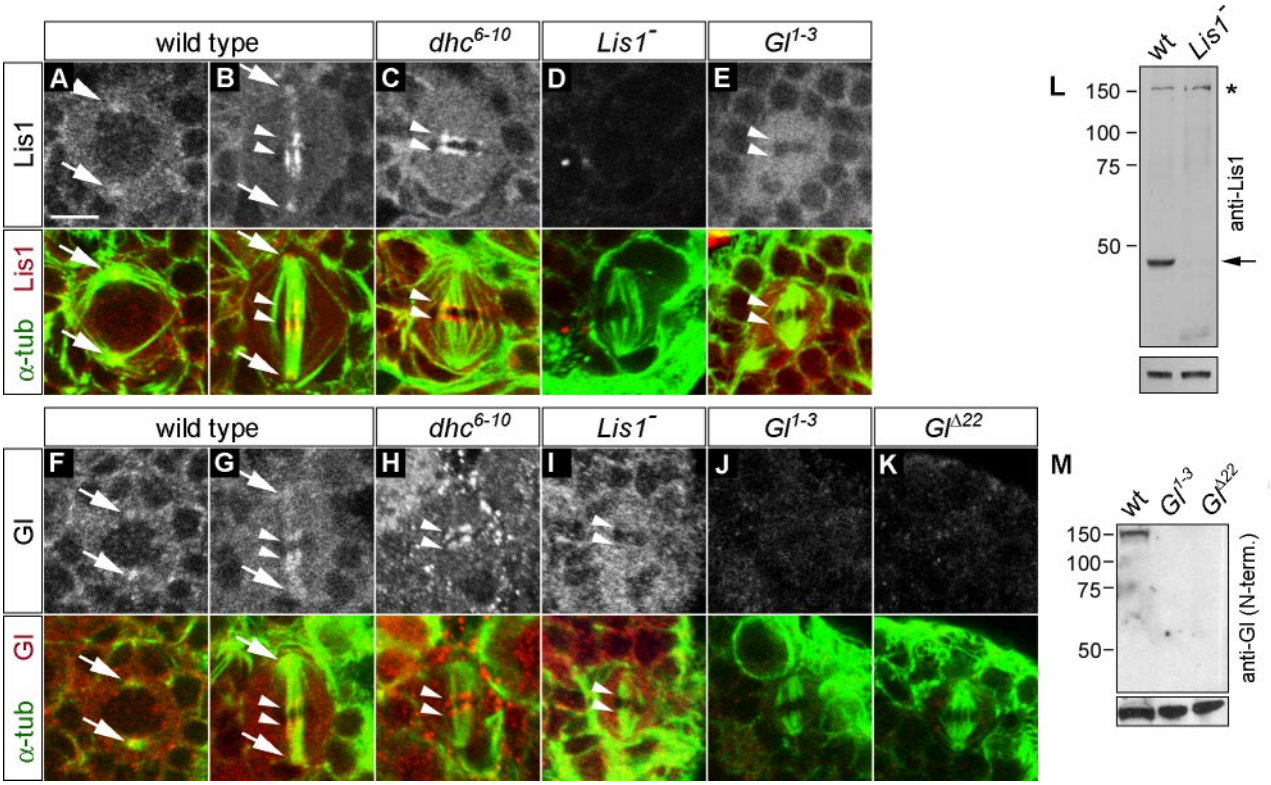

Figure 9. Lis1 and Gl protein localize to spindle poles/centrosomes, kinetochores, and spindle microtubules. (A–K) Neuroblasts of wild-type (A, B, F, and G), *dhc*$^{6-10}$ (C and H), *Lis1*$^{-}$ (D and I), *Gl*$^{1-3}$ (E and J), and *Gl*$^{\Delta 22}$ (K) mutant larvae were double-labeled for α-tubulin and Lis1 (A–E) or α-tubulin and Gl (antibody raised against Gl carboxy-terminus; Waterman-Storer and Holzbaur, 1996; F–K). Spindle poles/centrosomes (arrows) and kinetochores/kMTs (arrowheads) are indicated. Lis1 and Gl protein levels are reduced to background levels in *Lis1*$^{-}$ and *Gl* mutant metaphase neuroblasts, respectively, demonstrating the specificity of the Lis1 and Gl antibodies (D, J, and K). Bar, 5 μm. (L) Lis1 protein (~45 kDa) is almost undetectable in lysates of 2nd instar *Lis1*$^{-}$ mutant larvae compared with those of similarly aged wild-type (wt) larvae (arrow). Bottom panel: α-tubulin as loading control. The Lis1 antibody unspecifically detects a band of ~150 kDa (asterisk); this cross reactivity is unlikely to interfere with the Lis1 localization in neuroblasts as signals obtained with this antibody are reduced to background levels in *Lis1*$^{-}$ mutant neuroblasts (D). (M) Gl protein is undetectable in *Gl*$^{1-3}$ and *Gl*$^{\Delta 22}$ 2nd instar larval lysates using an antibody raised against the Gl amino-terminus (Fan and Ready, 1997). Bottom panel: α-tubulin as loading control.

that high cytoplasmic levels masked low levels of Lis1/dynactin at these sites. Thus, it remains unclear how Lis1/Gl promotes centrosome separation in neuroblasts. We found that centrosome separation was not completely blocked in *Lis1* or *Gl* mutant neuroblasts, either because of residual amounts of maternal protein or because of the presence of a Lis1/dynactin/dynein-independent pathway. Interestingly, cortical nonmuscle myosin II has recently been shown to contribute to centrosome separation in some cell types (Rosenblatt *et al.*, 2004), raising the possibility that Lis1/dynactin/dynein and myosin II play partially redundant roles in neuroblast centrosome separation.

Our observations further support a role for centrosomal/spindle pole-associated Lis1/Gl in spindle assembly, spindle pole focusing, and centrosome attachment in prometaphase and metaphase neuroblasts (summarized in Figure 11A). Detachment of centrosomes from the spindle has previously been observed in *dynein* mutants in *Drosophila* (Robinson *et*

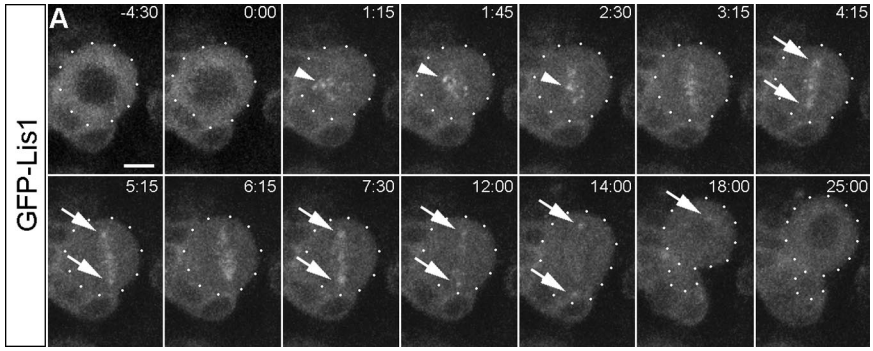

Figure 10. Dynamics of GFP-Lis1 protein localization in live neuroblasts. (A) GFP-Lis1 protein was expressed in wild-type 3rd instar larval brains (Supplementary Movie 10). Shortly after NEB, GFP-Lis1 protein was recruited into dotlike accumulations, likely reflecting kinetochore association (1:15, arrowhead). During metaphase GFP-Lis1 redistributed along spindle microtubules and became enriched on spindle poles (4:15–7:30, arrows). During anaphase and telophase (14:00–18:00) elevated levels of GFP-Lis1 were only detectable on spindle poles (arrow); only the apical spindle pole is in focus at 18:00. Mitosis was slightly delayed in these neuroblasts, presumably because of higher laser intensities used to visualize the GFP-Lis1 fusion protein. Bar, 5 μm.

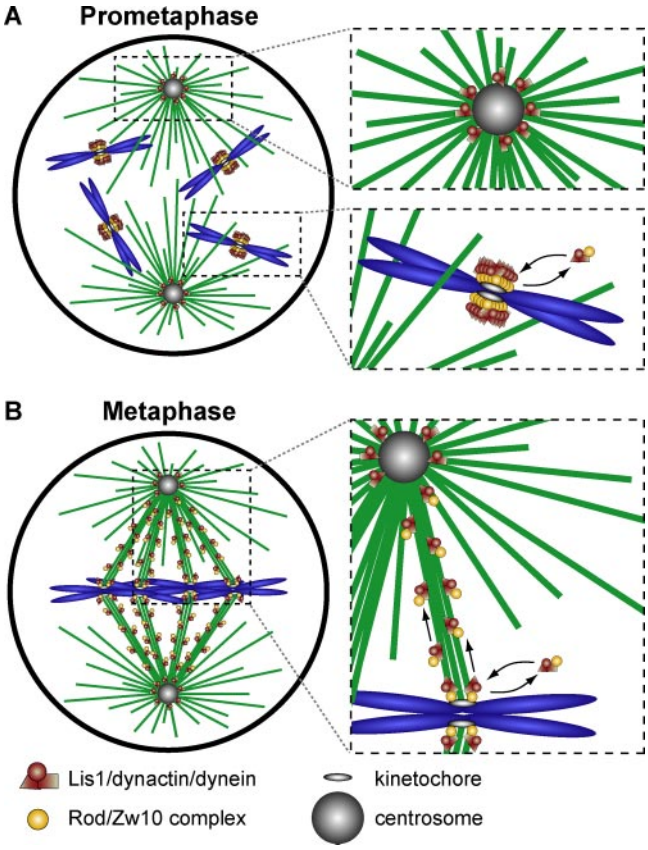

Figure 11. Summary of Lis1/dynactin localization in mitotic *Drosophila* neuroblasts. (A) During mitosis, Lis1/dynactin/dynein are enriched at centrosomes/spindle poles where they function in spindle pole focusing and centrosome attachment. During prometaphase, Lis1/dynactin are recruited to unattached kinetochores through binding to the Rod/Zw10 complex (we cannot rule out preassembly of a Lis1/dynactin/dynein-Rod/Zw10 complex in the cytoplasm). Lis1/dynactin/dynein may shuttle between kinetochores and cytoplasm as previously shown for Rod (Basto *et al.,* 2004). (B) At metaphase, after MT-attachment, kinetochore-bound Lis1/dynactin/dynein is associated with kMTs. It is required for transport of Rod (and possibly other checkpoint proteins) toward spindle poles. Checkpoint components may also shuttle between cytosol and kinetochores (Basto *et al.,* 2004; Howell *et al.,* 2004; Shah *et al.,* 2004). In addition, kinetochore-bound and/or spindle-associated Lis1/dynactin/dynein contribute to generation of interkinetochore-tension on bipolarly attached chromatid pairs. Both checkpoint protein transport and generation of interkinetochore tension may contribute to efficient checkpoint inactivation.

al., 1999; Wojcik *et al.,* 2001), and in mammalian cells with reduced dynein or dynactin function (Quintyne *et al.,* 1999). These findings, together with our results, show that Lis1 and dynactin act as cofactors for dynein-dependent focusing of spindle poles and attachment of spindle MTs minus-ends to centrosomes. In vertebrate cells dynein/dynactin is thought to contribute to focusing of spindle poles and attaching MT-minus ends to centrosomes by transporting pericentriolar proteins and MT-binding proteins, such as NuMA, to centrosomes (reviewed in Wittmann *et al.,* 2001; Blagden and Glover, 2003). Although no clear NuMA orthologue is encoded in the *Drosophila* genome, a dynein/dynactin/Lis1 complex may contribute to spindle pole focusing by concentrating other MT cross-linking proteins with NuMA-like function at spindle MT minus ends.

We found that *Gl* and *Lis1* mutant neuroblasts occasionally formed multipolar spindles and had more than two centrosomelike Centrosomin/γ-tubulin structures. Because of the lack of *Drosophila* centriolar markers we were not able to determine whether these extracentrosome-like structures contained centrioles. Multipolar spindles have also been observed in mammalian cells overexpressing Lis1 protein or in which Lis1 function was reduced (Faulkner *et al.,* 2000). Our time-lapse analysis of *Lis1* mutant neuroblasts revealed occasional cosegregation of both centrosomes into the neuroblast as a consequence of incomplete centrosome separation and centrosome detachment from the spindle. Such a mis-segregation event may be followed by duplication of both centrosomes during the next cell cycle, leading to supernumerary centrosomes. Alternatively, extracentrosomes in *Lis1* and *Gl* mutant neuroblasts may be due to uncoupling of centrosome duplication from the cell cycle or centrosome fragmentation.

The Role of Lis1/Dynactin in Regulating Cell Cycle Timing and Mitotic Checkpoint Signaling

Our time-lapse imaging experiments showed that loss of *Lis1/Gl* in neuroblasts results in extension of both prometaphase and metaphase. Prometaphase in *Lis1* mutant neuroblasts was characterized by delayed congression of chromosomes to the equatorial plate, which is likely to be largely due to inefficient kinetochore capturing as an indirect result of spindle assembly defects. Importantly, in *Lis1* mutant neuroblasts congression of all chromosomes into a tight metaphase plate eventually occurred, suggesting that Lis1/Gl are not absolutely critical for MT/kinetochore attachment per se.

In addition we observed severe delays in metaphase-to-anaphase transition. A few of these neuroblasts showed individual chromosomes that were transiently lost from and recongressed to the metaphase plate. Thus, consistent with findings in mammalian cells (Faulkner *et al.,* 2000), Lis1 appears to play some role in maintaining stable chromosome alignment in metaphase neuroblasts. However, in contrast to Faulkner *et al.* (2000), we found that loss of Lis1 function caused delays in metaphase-to-anaphase transition even when all chromosomes stayed aligned in a tight metaphase plate. Thus, mitotic checkpoint activity remained high even after apparent bipolar kinetochore attachment. Two defects appear to contribute to prolonged checkpoint activity in *Lis1* mutant metaphase neuroblasts: reduced interkinetochore tension and failure to transport checkpoint proteins (e.g., Rod) off kinetochores. Reduced interkinetochore tension may be due to lack of Lis1/dynactin on kinetochores or on spindle pole/MTs (which may affect forces acting on kinetochore pairs as a consequence of altered spindle morphology or MT dynamics). Defects in Rod checkpoint protein transport off kinetochores can be explained as a direct consequence of depletion of kinetochore-associated Lis1/dynactin/dynein motor complex, which in wild-type cells is loaded with Rod at kinetochores. However, previous studies indicated that Rod and Zw10 are removed from kinetochores in response to interkinetochore tension not MT attachment (Williams *et al.,* 1996; Scaerou *et al.,* 2001; Basto *et al.,* 2004). Therefore, in addition to its direct role as a "carrier," Lis1/dynactin/dynein may also play an indirect role in modulating Rod transport by generating the interkinetochore tension required to trigger initiation of Rod streaming.

In summary, our data are consistent with and extends a model recently proposed for dynein function in checkpoint protein transport in *Drosophila* and mammalian cells (Howell *et al.,* 2001; Wojcik *et al.,* 2001; Basto *et al.,* 2004). Accord-

ing to this model a Lis1/dynactin/dynein-Rod/Zw10 complex, preassembled on unattached kinetochores, is critical for timely anaphase onset by promoting poleward streaming of checkpoint proteins away from kinetochores after correct kinetochore-MT attachment has occurred (Figure 11B). Our data demonstrate that in *Drosophila*, the Lis1 protein is an obligate component in this process. Although the Lis1-binding proteins NudE/Nudel have been implicated in facilitating dynein-dependent checkpoint protein transport (Yan *et al.*, 2003), it remains to be directly tested whether Lis1 has a similar function in mammalian cells.

What is the link between Rod/Zw10 and Mad2 in mitotic checkpoint function? Two recent studies demonstrated that the Rod/Zw10 complex is required for efficient recruitment of Mad2 to unattached kinetochores in mammalian cells and *Drosophila* neuroblasts (Buffin *et al.*, 2005; Kops *et al.*, 2005) and that Mad2 and Rod colocalize during poleward transport along kMTs in *Drosophila* neuroblasts (Buffin *et al.*, 2005). Although a physical link between the Rod/Zw10 complex and Mad2 has not been discovered, an attractive model is that Rod/Zw10 links Mad2 to the Lis1/dynactin/dynein complex during poleward checkpoint protein transport (Buffin *et al.*, 2005; Kops *et al.*, 2005).

Epistasis of Lis1/Dynactin Localization at Kinetochores

Lis1/dynactin localization is regulated differently in worm and mammalian cells. In mammalian cells, dynactin is required for Lis1 kinetochore association, but Lis1 is not required for dynactin localization (Coquelle *et al.*, 2002; Tai *et al.*, 2002), whereas in *C. elegans*, Lis1 localizes to kinetochores independently of dynactin (Cockell *et al.*, 2004). Surprisingly, we find a third mechanism in *Drosophila* neuroblasts, where Lis1 and dynactin (Gl) are codependent for their localization to kinetochores. In neuroblasts, Lis1 may have a "structural" role in recruiting dynein/dynactin to the kinetochore, in addition to stimulating dynein/dynactin activity. Thus, despite the conservation of the physical interaction between Lis1/dynein/dynactin, subcellular localization of these proteins can be regulated differently in various organisms.

ACKNOWLEDGMENTS

We are grateful to Drs. Douglas Kankel, Don Ready, Roger Karess, Erika Holzbaur, Thomas Kaufman, Liqun Luo, Xavier Morin, Gary Karpen, Steve Henikoff, Robert Saint, and the Bloomington Stock Center for sharing reagents and fly lines. We especially thank Dr. Roger Karess for communicating results before publication, Sarah Siegrist for her help in developing the time-lapse imaging technique in larval brain explants, Amy Sheehan and Dr. Melissa Rolls for generating the pUAST-3xEmeraldGFP construct, Susie Shrimpton and Laurina Manning for technical assistance, and Sarah Siegrist as well as Drs. Stephan Schneider, Julie Canman, Bruce Bowerman, and Roger Karess for stimulating discussions. This work was supported by the American Heart Association (predoctoral fellowship to K.H.S.), the National Institutes of Health (Grant GM 053695 to T.S.H.), and the Howard Hughes Medical Institute (where C.Q.D. is an Investigator).

REFERENCES

Albertson, R., Chabu, C., Sheehan, A., and Doe, C. Q. (2004). Scribble protein domain mapping reveals a multistep localization mechanism and domains necessary for establishing cortical polarity. J. Cell Sci. *117*, 6061–6070.

Basto, R., Gomes, R., and Karess, R. E. (2000). Rough deal and Zw10 are required for the metaphase checkpoint in *Drosophila.* Nat. Cell Biol. *2*, 939–943.

Basto, R., Scaerou, F., Mische, S., Wojcik, E., Lefebvre, C., Gomes, R., Hays, T., and Karess, R. (2004). In vivo dynamics of the rough deal checkpoint protein during *Drosophila* mitosis. Curr. Biol. *14*, 56–61.

Bellen, H. J. *et al.* (2004). The BDGP gene disruption project: single transposon insertions associated with 40% of *Drosophila* genes. Genetics *167*, 761–781.

Blagden, S. P., and Glover, D. M. (2003). Polar expeditions—provisioning the centrosome for mitosis. Nat. Cell Biol. *5*, 505–511.

Buffin, E., Lefebvre, C., Huang, J., Gagou, M. E., and Karess, R. E. (2005). Recruitment of Mad2 to the kinetochore requires the Rod/Zw10 complex. Curr. Biol. *15*, 856–861.

Chan, G. K., Jablonski, S. A., Starr, D. A., Goldberg, M. L., and Yen, T. J. (2000). Human Zw10 and ROD are mitotic checkpoint proteins that bind to kinetochores. Nat. Cell Biol. *2*, 944–947.

Clarkson, M., and Saint, R. (1999). A His2AvDGFP fusion gene complements a lethal His2AvD mutant allele and provides an in vivo marker for *Drosophila* chromosome behavior. DNA Cell Biol. *18*, 457–462.

Cleveland, D. W., Mao, Y., and Sullivan, K. F. (2003). Centromeres and kinetochores: from epigenetics to mitotic checkpoint signaling. Cell *112*, 407–421.

Cockell, M. M., Baumer, K., and Gonczy, P. (2004). lis-1 is required for dynein-dependent cell division processes in *C. elegans* embryos. J. Cell Sci. *117*, 4571–4582.

Coquelle, F. M. *et al.* (2002). LIS1, CLIP-170's key to the dynein/dynactin pathway. Mol. Cell. Biol. *22*, 3089–3102.

Echeverri, C. J., Paschal, B. M., Vaughan, K. T., and Vallee, R. B. (1996). Molecular characterization of the 50-kD subunit of dynactin reveals function for the complex in chromosome alignment and spindle organization during mitosis. J. Cell Biol. *132*, 617–633.

Fan, S. S., and Ready, D. F. (1997). Glued participates in distinct microtubule-based activities in *Drosophila* eye development. Development *124*, 1497–1507.

Faulkner, N. E., Dujardin, D. L., Tai, C. Y., Vaughan, K. T., O'Connell, C. B., Wang, Y., and Vallee, R. B. (2000). A role for the lissencephaly gene LIS1 in mitosis and cytoplasmic dynein function. Nat. Cell Biol. *2*, 784–791.

Feng, Y., and Walsh, C.A. (2001). Protein-protein interactions, cytoskeletal regulation and neuronal migration. Nat. Rev. Neurosci. *2*, 408–416.

Fleming, S. L., and Rieder, C. L. (2003). Flattening *Drosophila* cells for high-resolution light microscopic studies of mitosis in vitro. Cell Motil. Cytoskelet. *56*, 141–146.

Gepner, J., Li, M., Ludmann, S., Kortas, C., Boylan, K., Iyadurai, S. J., McGrail, M., and Hays, T. S. (1996). Cytoplasmic dynein function is essential in *Drosophila melanogaster*. Genetics *142*, 865–878.

Gonczy, P., Pichler, S., Kirkham, M., and Hyman, A. A. (1999). Cytoplasmic dynein is required for distinct aspects of MTOC positioning, including centrosome separation, in the one cell stage *Caenorhabditis elegans* embryo. J. Cell Biol. *147*, 135–150.

Harte, P. J., and Kankel, D. R. (1982). Genetic analysis of mutations at the Glued locus and interacting loci in *Drosophila melanogaster*. Genetics *101*, 477–501.

Henikoff, S., Ahmad, K., Platero, J. S., and van Steensel, B. (2000). Heterochromatic deposition of centromeric histone H3-like proteins. Proc. Natl. Acad. Sci. USA *97*, 716–721.

Heuer, J. G., Li, K., and Kaufman, T. C. (1995). The *Drosophila* homeotic target gene centrosomin (cnn) encodes a novel centrosomal protein with leucine zippers and maps to a genomic region required for midgut morphogenesis. Development *121*, 3861–3876.

Howell, B. J., Hoffman, D. B., Fang, G., Murray, A. W., and Salmon, E. D. (2000). Visualization of Mad2 dynamics at kinetochores, along spindle fibers, and at spindle poles in living cells. J. Cell Biol. *150*, 1233–1250.

Howell, B. J., McEwen, B. F., Canman, J. C., Hoffman, D. B., Farrar, E. M., Rieder, C. L., and Salmon, E. D. (2001). Cytoplasmic dynein/dynactin drives kinetochore protein transport to the spindle poles and has a role in mitotic spindle checkpoint inactivation. J. Cell Biol. *155*, 1159–1172.

Howell, B. J., Moree, B., Farrar, E. M., Stewart, S., Fang, G., and Salmon, E. D. (2004). Spindle checkpoint protein dynamics at kinetochores in living cells. Curr. Biol. *14*, 953–964.

Hoyt, M. A., Totis, L., and Roberts, B. T. (1991). *S. cerevisiae* genes required for cell cycle arrest in response to loss of microtubule function. Cell *66*, 507–517.

Irion, U., Leptin, M., Siller, K., Fuerstenberg, S., Cai, Y., Doe, C. Q., Chia, W., and Yang, X. (2004). Abstrakt, a DEAD box protein, regulates Insc levels and asymmetric division of neural and mesodermal progenitors. Curr. Biol. *14*, 138–144.

Karess, R. E., and Glover, D. M. (1989). rough deal: a gene required for proper mitotic segregation in *Drosophila.* J. Cell Biol. *109*, 2951–2961.

Karki, S., and Holzbaur, E. L. (1999). Cytoplasmic dynein and dynactin in cell division and intracellular transport. Curr. Opin. Cell Biol. *11*, 45–53.

Kiehart, D. P., Montague, R. A., Rickoll, L., Thomas, G. L., and Foard, D. (1994). High-resolution microscopic methods for the analysis of cellular movements in *Drosophila* embryos. In: *Drosophila melanogaster*: Practical Uses in Cellular and Molecular Biology, vol. 44, ed. L.S.B. Goldstein and E. A. Fyrberg, San Diego: Academic Press, 507–532.

King, S. J., and Schroer, T. A. (2000). Dynactin increases the processivity of the cytoplasmic dynein motor. Nat. Cell Biol. *2*, 20–24.

Kops, G. J., Kim, Y., Weaver, B. A., Mao, Y., McLeod, I., Yates, J. R., 3rd, Tagaya, M., and Cleveland, D. W. (2005). ZW10 links mitotic checkpoint signaling to the structural kinetochore. J. Cell Biol. *169*, 49–60.

Li, R., and Murray, A. W. (1991). Feedback control of mitosis in budding yeast. Cell *66*, 519–531.

Li, X., and Nicklas, R. B. (1995). Mitotic forces control a cell-cycle checkpoint. Nature *373*, 630–632.

Liu, Z., Xie, T., and Steward, R. (1999). Lis1, the *Drosophila* homolog of a human lissencephaly disease gene, is required for germline cell division and oocyte differentiation. Development *126*, 4477–4488.

McGrail, M., and Hays, T. S. (1997). The microtubule motor cytoplasmic dynein is required for spindle orientation during germline cell divisions and oocyte differentiation in *Drosophila.* Development *124*, 2409–2419.

Morin, X., Daneman, R., Zavortink, M., and Chia, W. (2001). A protein trap strategy to detect GFP-tagged proteins expressed from their endogenous loci in *Drosophila.* Proc. Natl. Acad. Sci. USA *98*, 15050–15055.

Pfarr, C. M., Coue, M., Grissom, P. M., Hays, T. S., Porter, M. E., and McIntosh, J. R. (1990). Cytoplasmic dynein is localized to kinetochores during mitosis. Nature *345*, 263–265.

Quintyne, N. J., Gill, S. R., Eckley, D. M., Crego, C. L., Compton, D. A., and Schroer, T. A. (1999). Dynactin is required for microtubule anchoring at centrosomes. J. Cell Biol. *147*, 321–334.

Reiner, O., Carrozzo, R., Shen, Y., Wehnert, M., Faustinella, F., Dobyns, W. B., Caskey, C. T., and Ledbetter, D. H. (1993). Isolation of a Miller-Dieker lissencephaly gene containing G protein beta-subunit-like repeats. Nature *364*, 717–721.

Rieder, C. L., Cole, R. W., Khodjakov, A., and Sluder, G. (1995). The checkpoint delaying anaphase in response to chromosome monoorientation is mediated by an inhibitory signal produced by unattached kinetochores. J. Cell Biol. *130*, 941–948.

Robinson, J. T., Wojcik, E. J., Sanders, M. A., McGrail, M., and Hays, T. S. (1999). Cytoplasmic dynein is required for the nuclear attachment and migration of centrosomes during mitosis in *Drosophila.* J. Cell Biol. *146*, 597–608.

Rosenblatt, J., Cramer, L. P., Baum, B., and McGee, K. M. (2004). Myosin II-dependent cortical movement is required for centrosome separation and positioning during mitotic spindle assembly. Cell *117*, 361–372.

Savoian, M. S., and Rieder, C. L. (2002). Mitosis in primary cultures of *Drosophila melanogaster* larval neuroblasts. J. Cell Sci. *115*, 3061–3072.

Scaerou, F., Aguilera, I., Saunders, R., Kane, N., Blottiere, L., and Karess, R. (1999). The rough deal protein is a new kinetochore component required for accurate chromosome segregation in *Drosophila.* J. Cell Sci. *112*(Pt 21), 3757–3768.

Scaerou, F., Starr, D. A., Piano, F., Papoulas, O., Karess, R. E., and Goldberg, M. L. (2001). The ZW10 and Rough Deal checkpoint proteins function together in a large, evolutionarily conserved complex targeted to the kinetochore. J. Cell Sci. *114*, 3103–3114.

Schmidt, D. J., Rose, D. J., Saxton, W. M., and Strome, S. (2005). Functional analysis of cytoplasmic dynein heavy chain in *Caenorhabditis elegans* with fast-acting temperature-sensitive mutations. Mol. Biol. Cell *16*, 1200–1212.

Schroer, T. A. (2004). Dynactin. Annu. Rev. Cell Dev. Biol. *20*, 759–779.

Shah, J. V., Botvinick, E., Bonday, Z., Furnari, F., Berns, M., and Cleveland, D. W. (2004). Dynamics of centromere and kinetochore proteins; implications for checkpoint signaling and silencing. Curr. Biol. *14*, 942–952.

Smith, D. S., Niethammer, M., Ayala, R., Zhou, Y., Gambello, M. J., Wynshaw-Boris, A., and Tsai, L. H. (2000). Regulation of cytoplasmic dynein behaviour and microtubule organization by mammalian Lis1. Nat. Cell Biol. *2*, 767–775.

Starr, D. A., Williams, B. C., Hays, T. S., and Goldberg, M. L. (1998). ZW10 helps recruit dynactin and dynein to the kinetochore. J. Cell Biol. *142*, 763–774.

Starr, D. A., Williams, B. C., Li, Z., Etemad-Moghadam, B., Dawe, R. K., and Goldberg, M. L. (1997). Conservation of the centromere/kinetochore protein ZW10. J. Cell Biol. *138*, 1289–1301.

Steuer, E. R., Wordeman, L., Schroer, T. A., and Sheetz, M. P. (1990). Localization of cytoplasmic dynein to mitotic spindles and kinetochores. Nature *345*, 266–268.

Tai, C. Y., Dujardin, D. L., Faulkner, N. E., and Vallee, R. B. (2002). Role of dynein, dynactin, and CLIP-170 interactions in LIS1 kinetochore function. J. Cell Biol. *156*, 959–968.

Taylor, S. S., Scott, M. I., and Holland, A. J. (2004). The spindle checkpoint: a quality control mechanism which ensures accurate chromosome segregation. Chromosome Res. *12*, 599–616.

Tsien, R. Y. (1998). The green fluorescent protein. Annu. Rev. Biochem. *67*, 509–544.

Vaisberg, E. A., Koonce, M. P., and McIntosh, J. R. (1993). Cytoplasmic dynein plays a role in mammalian mitotic spindle formation. J. Cell Biol. *123*, 849–858.

Vallee, R. B., Tai, C., and Faulkner, N. E. (2001). LIS1, cellular function of a disease-causing gene. Trends Cell Biol. *11*, 155–160.

Waterman-Storer, C. M., and Holzbaur, E. L. (1996). The product of the *Drosophila* gene, Glued, is the functional homologue of the p150Glued component of the vertebrate dynactin complex. J. Biol. Chem. *271*, 1153–1159.

Waters, J. C., Cole, R. W., and Rieder, C. L. (1993). The force-producing mechanism for centrosome separation during spindle formation in vertebrates is intrinsic to each aster. J. Cell Biol. *122*, 361–372.

Williams, B. C., Gatti, M., and Goldberg, M. L. (1996). Bipolar spindle attachments affect redistributions of ZW10, a *Drosophila* centromere/kinetochore component required for accurate chromosome segregation. J. Cell Biol. *134*, 1127–1140.

Williams, B. C., Karr, T. L., Montgomery, J. M., and Goldberg, M. L. (1992). The *Drosophila* l(1)zw10 gene product, required for accurate mitotic chromosome segregation, is redistributed at anaphase onset. J. Cell Biol. *118*, 759–773.

Williams, B. C., Li, Z., Liu, S., Williams, E. V., Leung, G., Yen, T. J., and Goldberg, M. L. (2003). Zwilch, a new component of the ZW10/ROD complex required for kinetochore functions. Mol. Biol. Cell *14*, 1379–1391.

Wittmann, T., Hyman, A., and Desai, A. (2001). The spindle: a dynamic assembly of microtubules and motors. Nat. Cell Biol. *3*, E28–E34.

Wojcik, E., Basto, R., Serr, M., Scaerou, F., Karess, R., and Hays, T. (2001). Kinetochore dynein: its dynamics and role in the transport of the Rough deal checkpoint protein. Nat. Cell Biol. *3*, 1001–1007.

Yan, X., Li, F., Liang, Y., Shen, Y., Zhao, X., Huang, Q., and Zhu, X. (2003). Human Nudel and NudE as regulators of cytoplasmic dynein in poleward protein transport along the mitotic spindle. Mol. Cell. Biol. *23*, 1239–1250.